



Contents lists available at ScienceDirect

Journal of Molecular Spectroscopy

journal homepage: www.elsevier.com/locate/jmsThe rotational spectra of the 6^1 , 7^1 , 8^1 , 9^1 and $5^1/9^2$ vibrational states of H^{15}NO_3 Douglas T. Petkie^{a,*}, Mark Kipling^a, Ashley Jones^a, Paul Helminger^b, Ivan R. Medvedev^c, Atsuko Maeda^c, Markus Behnke^{c,1}, Brian J. Drouin^d, Charles E. Miller^d^a Department of Physics, Wright State University, 248 Fawcett Hall, 3640 Colonel Glenn Hwy, Dayton, OH 45435, USA^b Department of Physics, University of South Alabama, Mobile, AL 36688, USA^c Department of Physics, Ohio State University, Columbus, OH 43210, USA^d Jet Propulsion Laboratory, California Institute of Technology, Pasadena, CA 91109, USA

ARTICLE INFO

Article history:

Received 15 February 2008

In revised form 24 March 2008

Available online 9 April 2008

Keywords:

Nitric acid

Isotope

Rotational spectroscopy

Torsional splitting

Coriolis resonance

Fermi resonance

Centrifugal distortion

ABSTRACT

The high-resolution rotational spectrum of H^{15}NO_3 has been recorded in the range between 74 and 850 GHz and used to complete an extensive analysis of the six vibrational states below 1000 cm^{-1} that include the isolated 8^1 and 9^1 states along with the weakly interacting 6^1 and 7^1 states and strongly interacting 5^1 and 9^2 dyad. The 6^1 and 7^1 states couple via a weak Coriolis interaction while the 5^1 and 9^1 states couple through strong Fermi and weaker Coriolis interactions. The Hamiltonian models account for the observed torsional splitting in the 9^1 and 9^2 states of 2.4 and 70 MHz, respectively, and the induced torsional splitting of 15 MHz in the 5^1 state due to the strong Fermi mixing with the 9^2 state. The transitions from each state are fit to within the experimental accuracy and the resulting spectroscopic constants agree well with the main isotopologue.

© 2008 Elsevier Inc. All rights reserved.

1. Introduction

Spectroscopic characterization of nitric acid (HNO_3) continues to be a focus of laboratory studies since it is an important atmospheric trace gas and critical for understanding stratospheric ozone depletion chemistry [1]. Accurate HNO_3 concentration profiles retrieved via remote sensing, such as from NASA's MLS instruments on Aura and UARS or ESA's MIPAS instrument aboard ENVISAT, depend on the complete understanding of the spectroscopic details of HNO_3 . As the sensitivity of the retrievals from these and future satellite instruments increases, the weaker spectra of transitions from vibrationally excited states and less abundant isotopologues of HNO_3 will interfere with the detection of the normal species and will need to be accurately modeled to remove systematic errors in the retrieved concentration profiles. Perrin et al. [2] recently reported the detection of H^{15}NO_3 in the atmosphere (fractional abundance of 0.003663(4) [3]) by identifying the ν_5 Q-branch near 871 cm^{-1} in the residuals of the fitted MIPAS spectra and H^{15}NO_3 spectral interference likely exists in other regions currently used to retrieve atmospheric nitric acid.

Several ground state rotational transitions of H^{15}NO_3 were first measured by Millen and Morton [4] in the microwave region and

recently extended into the submillimeter wave region by Drouin et al. [5], providing a well determined set of ground state rotational and centrifugal distortional constants for H^{15}NO_3 . The low resolution infrared spectrum was measured by McGraw et al. [6] and used to determine the band origins of the fundamental vibrations. High resolution infrared studies include those for the ν_2 band [7], the four lowest fundamental bands ν_9 , ν_7 , ν_6 , and ν_8 [8], and the strongly interacting ν_5 and $2\nu_9$ bands [9]. In the latter study of the 5^1 and 9^2 states, Perrin et al. [9] observed an intensity ratio between the $2\nu_9$ and ν_5 bands of $\text{Int}(2\nu_9)/\text{Int}(\nu_5) \sim 0.23$ that was satisfactorily explained by the weaker $2\nu_9$ band borrowing intensity from the stronger ν_5 band via a strong Fermi resonance. This result was based on the use of the previously determined F_0 Fermi parameter for the main isotopologue [10] and was not fit for in the H^{15}NO_3 infrared analysis. The torsional splitting was not large enough to be resolved in the infrared spectrum for either state.

This paper reports an analysis of the H^{15}NO_3 rotational spectrum recorded in the 74–850 GHz frequency range and includes all excited vibrational states with bands origins below 1000 cm^{-1} : $\nu_9 = 1$, $\nu_7 = 1$, $\nu_6 = 1$, $\nu_8 = 1$, $\nu_5 = 1$, and $\nu_9 = 2$. The fits include Coriolis coupling (ν_6/ν_7), Coriolis and Fermi interactions ($\nu_5/2\nu_9$) and torsional splitting (ν_9 , ν_5 , $2\nu_9$). The analysis method and Hamiltonians used in the present work follow closely those used for the analysis of the H^{14}NO_3 parent isotopologue [10–13]. The most recent analyses of the ground and four lowest vibrational states of H^{14}NO_3 were updated in Ref. [11]. Refs. [10,12] provide

* Corresponding author. Fax: +1 937 775 2222.

E-mail address: doug.petkie@wright.edu (D.T. Petkie).¹ Present address: German Research Foundation, 53175 Bonn, Germany.

details of the Hamiltonian that describes the strong Fermi and Coriolis interactions between the 5^1 and 9^2 vibrational states as well as models for the torsional splitting. Ref. [13] provides details of the weak Coriolis interaction between the 6^1 and 7^1 vibrational state that was included to account for the systematic effect the interaction has on the quartic distortional constants. The H^{15}NO_3 data set and spectroscopic constants reported here are suitable for prediction of the observable millimeter and submillimeter wave spectrum as well as for simulating the infrared spectrum below 1000 cm^{-1} .

2. Experimental

The experimental data sets were collected from two different systems, the OSU FASSST and the JPL Frequency Multiplier Spectrometers. The OSU Fast Scan Submillimeter Spectroscopic Technique (FASSST) system is described in Refs. [14–16], and provided heated data over the frequency ranges from 118 to 186 GHz and 192 to 377 GHz using three different free-running, fast swept BWO tubes as sources and helium cooled hot-electron bolometers as detectors. The frequency was calibrated by use of separately recorded frequency markers from a cavity and SO_2 reference lines. An isotope enriched H^{15}NO_3 sample was purchased from ISOTECH and filled a 6 m long, 15 cm diameter aluminum cell to a pressure of ~ 10 m Torr that was maintained in a slow flow and heated to $\sim 170^\circ\text{C}$ to populate the higher lying vibrational states. A separate 60 cm cell in series with the sample cell was filled to ~ 10 m Torr with SO_2 that was used as a reference spectrum in order to calibrate the frequency. For most data sets, the normal species was only observed in small amounts ($\sim 5\%$ or less), however, for a few regions, the normal species was observed at concentrations of 50% that of the isotope concentration. In general,

this did not pose any problems since the spectrum of the normal species is well characterized in Refs. [11–13] and did not significantly interfere due to the isotopic shift in frequencies, as shown in Fig. 1. The estimated accuracy of the measured transitions is 50–100 kHz.

The JPL Frequency Multiplier Submillimeter Spectrometer (FMSS) is described in Ref. [17] and provided spectra over the ranges of 74–109, 402–420, 639–656, and 800–850 GHz. Using an isotope enriched sample (98%), a gas pressure of ~ 10 m Torr was maintained in a slow flow in a room temperature 2 m long cell. The microwave synthesizer driving the multiplier chain was frequency modulated and the spectrum was recorded at the 2nd harmonic with a lock-in amplifier after being detected with either a room temperature diode detector near 100 GHz or a helium cooled hot-electron bolometer at the higher frequencies. Line positions were measured to 50–100 kHz precision. All of the data from both spectrometers were equally weighted in the analyses with a 100 kHz uncertainty.

3. Observed spectra and analyses

Nitric acid is a planar oblate asymmetric rotor ($\kappa = 0.729$) belonging to the C_s point group with dipole moments of $\mu_a = 1.986D$ and $\mu_b = 0.882D$ [18]. The spectrum of each vibrational state is characterized by strong R-type band heads spaced by approximately 12.5 GHz throughout the spectrum along with much more broadly spaced Q-branch transitions. Since the isotopic substitution of the nitrogen atom is close to the center of mass, the transitions in the symmetric-top limit are only slightly shifted from the normal species. The initial assignments for each vibrational state were made in order of ascending band origin energy by using the predicted spectrum of the normal species and identi-

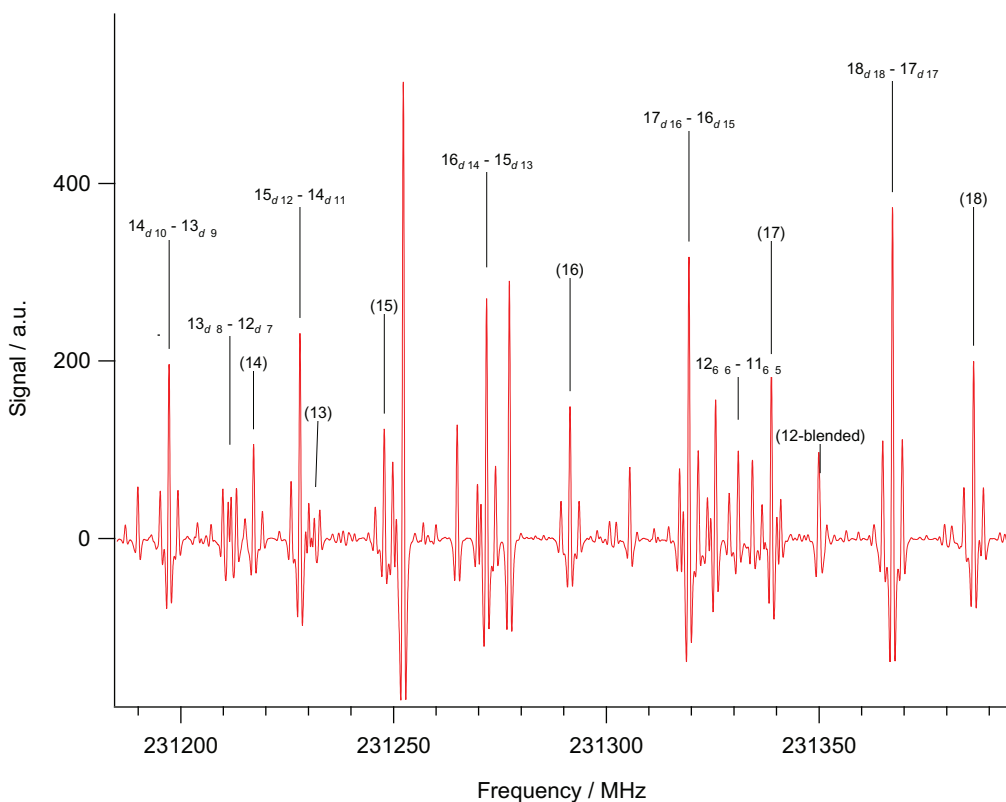


Fig. 1. The $\nu_9 = 1$ R-branch band heads for the H^{15}NO_3 and H^{14}NO_3 isotopologues near 231 GHz. The characteristic triplet torsional splitting pattern consists of degenerate *a*-type transitions with weaker *b*-type satellites split by ~ 2 MHz. The *a*-type transitions are identified with the quantum numbers given for the H^{15}NO_3 isotopologue, where $d = (J - K_a)$ and $(J - K_a + 1)$, and the J rotational quantum number is given in parenthesis for the H^{14}NO_3 isotopologue transitions.

fying R-band heads that were slightly shifted in frequency and had the appropriate intensity, as shown in Fig. 1. The analysis for each corresponding vibrational state of the normal species served as the starting point for each analysis, with higher order distortional constants initially frozen until the data set was expanded. In the end, four separate analyses describe the rotational spectra of six vibrational states that all have band origins below 1000 cm^{-1} . Of these four analyses, the 8^1 and 9^1 states were fit as isolated states. Since the 6^1 and 7^1 states exhibit a weak Coriolis interaction at high J and K_a , an interaction term was included in a joint analysis of these states. The 9^2 and 5^1 states are coupled via strong Fermi and weaker Coriolis interactions. The Fermi interaction results in a mixing of the vibrational wavefunctions, consequently the 5^1 level also exhibits a torsional splitting in the spectra. Watson's effective A -reduced Hamiltonian in the I' coordinate representation [19] was used in the analysis of the 8^1 , 6^1 and 7^1 states and was modified by using an internal axis system Hamiltonian with torsional parameters for the 9^1 , 5^1 and 9^2 states. All spectra were fit with

the JPL SPFIT/SPCAT program suite [20,21]. Maximum values of the J and K_a quantum numbers for this isotope exceeds those for the normal species due to the recent improvements in the FASSST system that increased the sensitivity with the implementation of new signal averaging routines [15].

3.1. 8^1 state analysis

The 8^1 state is free from any significant perturbations and does not exhibit a resolvable torsional splitting; consequently it can be described with the simplest Hamiltonian and is therefore presented first. The ν_8 vibrational mode corresponds to the NO_2 out of plane bend and is centered near 743.6 cm^{-1} , shifted up by less than 1 cm^{-1} from the main isotopologue [8,22]. Table 1 summarizes the measurements that include 715 transitions that extend to maximum quantum numbers of $J=72$ and $K_a=47$. As discussed in Ref. [13], several of the quartic distortional constants for the vibrational states of nitric acid can vary

Table 1
Spectroscopic constants for the 9^1 , 7^1 , 6^1 , 8^1 , 5^1 and 9^2 states of $\text{H}^{15}\text{NO}_3^a$

	$\nu_9 = 1$	$\nu_7 = 1$	$\nu_6 = 1$	$\nu_8 = 1$	$\nu_5 = 1$	$\nu_9 = 2$
ν_0/cm^{-1}	458.29167 ^b	578.47191 ^b	646.96407 ^b	743.61660 ^b	875.0731(14)	889.4783(14)
$\rho/\text{unitless}$	1.468285 ^c	[0.0]	[0.0]	[0.0]	1.46810 ^c	1.46810 ^c
E_ρ/MHz	1.213(3)	[0.0]	[0.0]	[0.0]	[0.0]	-43.0437(115)
$E_{\rho J}/\text{kHz}$	[0.0]	[0.0]	[0.0]	[0.0]	[0.0]	-1.6502(291)
$E_{\rho K}/\text{kHz}$	[0.0]	[0.0]	[0.0]	[0.0]	[0.0]	3.388(33)
$E_{\rho z}/\text{kHz}$	[0.0]	[0.0]	[0.0]	[0.0]	[0.0]	0.8180(74)
$E_{\rho D_{ab}}/\text{kHz}$	[0.0]	[0.0]	[0.0]	[0.0]	[0.0]	-0.2141(147)
$E_{\rho J^2}/\text{Hz}$	[0.0]	[0.0]	[0.0]	[0.0]	[0.0]	-0.1378(126)
A/MHz	12964.232(113)	13028.00561(167)	13006.98612(163)	13000.93720(42)	12961.3070(264)	12966.5713(164)
B/MHz	12047.920(113)	12096.17370(164)	12054.47426(162)	12003.82226(39)	12137.5114(260)	11966.7862(165)
C/MHz	6254.721229(270)	6242.62085(33)	6240.211998(310)	6260.29604(42)	6233.9663(116)	6248.6970(115)
D_{ab}/MHz	-185.064(279)	[0.0]	[0.0]	[0.0]	-210.220(50)	-171.419(49)
D_{abJ}/kHz	[0.0]	[0.0]	[0.0]	[0.0]	2.3790(262)	1.6896(245)
D_{abK}/kHz	-1.675(41)	[0.0]	[0.0]	[0.0]	-1.978(53)	-1.522(88)
Δ_J/kHz	8.69687(80)	9.216139(229)	9.410316(201)	8.93445(43)	9.1296(56)	9.0399(43)
Δ_{JK}/kHz	-3.7934(316)	-6.0589(134)	-4.4987(136)	-3.91647(69)	-5.416(50)	-4.642(54)
Δ_K/kHz	6.580(49)	8.8049(130)	6.6723(139)	6.48130(73)	6.989(91)	6.260(85)
δ_J/kHz	3.67298(40)	3.943867(103)	3.993078(118)	3.795301(117)	3.90064(281)	3.84203(215)
δ_K/kHz	7.1479(145)	8.0542(67)	7.6628(66)	6.888344(283)	8.2624(263)	7.2774(258)
Φ_J/Hz	-0.004270(38)	0.003226(39)	-0.011763(47)	0.014256(117)	[0.0]	-0.005834(174)
Φ_{JK}/Hz	-0.02242(54)	-0.02714(202)	0.12392(213)	-0.06375(41)	0.01178(172)	0.02697(205)
Φ_{KJ}/Hz	0.09787(184)	-0.05250(267)	-0.25286(243)	0.06997(63)	-0.01023(233)	-0.0126(79)
Φ_K/Hz	-0.04686(149)	0.11445(113)	0.17321(53)	0.01264(71)	[0.0]	0.0216(76)
ϕ_J/Hz	-0.0017775(182)	0.0020144(216)	-0.0054011(247)	0.007480(39)	-0.000168(54)	-0.002346(83)
ϕ_{JK}/Hz	-0.021435(226)	-0.02820(114)	0.03643(120)	0.000337(181)	-0.03441(84)	-0.00200(96)
ϕ_{KJ}/Hz	0.06032(46)	0.05084(37)	0.09132(33)	0.02807(34)	0.15773(119)	0.03691(266)
$L_{JK}/\mu\text{Hz}$	[0.0]	3.809(134)	[0.0]	4.494(277)	[0.0]	[0.0]
$L_{KJ}/\mu\text{Hz}$	[0.0]	[0.0]	[0.0]	-5.65(37)	[0.0]	[0.0]
$L_K/\mu\text{Hz}$	[0.0]	-3.576(208)	[0.0]	[0.0]	[0.0]	[0.0]
$l_{JK}/\mu\text{Hz}$	[0.0]	-1.485(55)	0.413(60)	[0.0]	[0.0]	[0.0]
$l_{KJ}/\mu\text{Hz}$	[0.0]	[0.0]	[0.0]	-1.505(84)	[0.0]	[0.0]
$l_K/\mu\text{Hz}$	1.891(76)	[0.0]	[0.0]	1.990(146)	[0.0]	[0.0]
			$\nu_7 = \leftrightarrow \nu_6 = 1$			$\nu_5 = 1 \leftrightarrow \nu_9 = 2$
C/MHz			[-9030]			[0.0]
C_{ab}/MHz			-41.941(181)			2.3060(195)
C_{abJ}/kHz			0.7642(272)			
C_{abK}/kHz						-0.1042(43)
F_a/MHz						256314(35)
F_J/MHz						-7.4236(100)
F_K/MHz						6.4871(174)
F_z/MHz						-3.2743(45)
$F_{\pm K}/\text{kHz}$						0.23496(111)
Number of transitions	1193	761	735	715	544 ^d	581 ^d
$J_{\text{max}}, K_{a\text{max}}, K_{c\text{max}}$	73, 59, 65	70, 50, 65	71, 50, 65	72, 47, 49	60, 41, 52	60, 40, 52
rms deviation/MHz	0.083	0.074	0.071	0.067	0.074	0.067

^a Numbers in parentheses are standard errors (1σ), enough digits are supplied to reproduce the observed spectra.

^b The band origins are from Ref. [8].

^c Parameter cannot be fit with SPFIT and was adjusted empirically to minimize the rms deviation.

^d 79 of the transitions were between the $\nu_5 = 1$ and $\nu_9 = 2$ states.

by more than 10% when compared to the ground state constants due to correlations in the constants and the chosen reduction (A or S) and representation (I' , III' , ...) of the Hamiltonian. For the analysis of the 8^1 state, Δ_{JK} , Δ_K and δ_K are shifted down by 17%, 14%, and 9%, respectively. However, when comparing the determinable combinations of coefficients (T_{aa} , T_{bb} , T_{cc} , T_1 and T_2 as given in Gordy and Cook [23]) the variation between the ground state and 8^1 quartic constants are all less than 6%. The T coefficients vary only slightly from the ground state and the *rms* deviation of the fitted lines is 67 kHz, which indicates that the 8^1 state does not have a significant perturbation over the set of measured transitions. These parameters are therefore a good diagnostic for determining the presence of interactions between the vibrational states of nitric acid.

3.2. 6^1 and 7^1 state analysis

The v_6 vibrational mode corresponds to the O–NO₂ stretch and is centered near 647 cm⁻¹, shifted up by less than 0.2 cm⁻¹ from the main isotopologue [8,24] and the v_7 vibrational mode corresponds to the O–NO₂ bend and is centered near 578.5 cm⁻¹, shifted down by less than 2 cm⁻¹ from the main isotopic species [8,22]. Table 1 summarizes the measurements that include 761 transitions that extend to maximum quantum numbers of $J = 70$ and $K_a = 50$ for the 7^1 state and 735 transitions that extend to maximum quantum numbers of $J = 71$ and $K_a = 50$ for the 6^1 state. The difference in the band origins is 68.5 cm⁻¹, so these two states are not expected to have significant perturbations. However, several Q-branch transitions in the frequency range from 275 to 375 GHz displayed a systematic deviation for quantum numbers $J \geq 58$ (to 71) and $K_c \geq 23$ (to 31) for the 7^1 state and $K_c \geq 24$ (to 31) for 6^1 state with approximately 20 transitions with deviations between 0.5 and 1.0 MHz and six transitions with deviation between 1.0 and 10.0 MHz. These deviations have been attributed to the Coriolis interaction and the effected transitions could not be fit to experimental accuracy without the inclusion of Coriolis parameters in the Hamiltonian. Inclusion of higher order distortional terms (a complete set of octic terms) in separate analyses that did not include the Coriolis coupling could not absorb the effect of the interaction.

As discussed in Ref. [13], differences in the T_{cc} coefficients for the 6^1 and 7^1 states indicated the presence of a C-type Coriolis interaction for the main isotopologue. In this work, when each state was fit separately, the T_{cc} coefficients differed from the ground state by 61% for the 6^1 state and -54% for the 7^1 state. The shift of the T_{cc} distortional coefficients due to the first-order Coriolis interaction was derived by Tanaka and Morino [25] and is given by

$$\Delta T_{cc} = \pm \frac{(G_{67}^c)^4}{(\omega_6 - \omega_7)^3}, \quad (1)$$

where the coupling coefficient is given by

$$G_{67}^c = \zeta_{67}^c C_e \frac{\omega_6 + \omega_7}{\sqrt{\omega_6 \omega_7}} \sqrt{(v_6 + 1)v_7} \quad (2)$$

and $y = c$ in the I' representation, ζ_{67}^c is the Coriolis coupling constant, C_e is the equilibrium rotational constant and ω_6 and ω_7 are the harmonic vibrational frequencies. Following the methodology in Ref. [13], the Coriolis coupling constant ζ_{67}^c was calculated using the difference in the T_{cc} coefficients (1.5369 kHz) from the separate, uncoupled 6^1 and 7^1 state analyses, the ground state rotational constant for C_e from Ref. [5] and the observed band origins for the ω_6 and ω_7 from Ref. [8]. Based on these parameters, the Coriolis coupling constant was calculated to be $\zeta_{67}^c = -0.720$, which allowed the coupling coefficient G_{67}^c to be calculated.

The off-diagonal vibrational Coriolis operators used in the Hamiltonian are given by

$$\langle v_6, v_7 | \mathbf{H}_{v_6 v_7}^c | v_6 + 1, v_7 - 1 \rangle = iG_{67}^c J_c + (C_{ab} + C_{ab} J^2) \{J_a, J_b\} + \frac{C_{ab} K}{2} \times \{J_a^2, \{J_a, J_b\}\}. \quad (3)$$

The first-order Coriolis term was fixed at the value determined by the above method since it is highly correlated with rotational and distortional constants and causes the analysis to be unstable. Two higher order terms were free parameters in the analysis and were determined. With the inclusion of the Coriolis parameters in the coupled state analysis, the T_{cc} coefficients differed from the ground state by 6.6% for the 6^1 state and -0.6% for the 7^1 state and all the transitions were fit to within 300 kHz with the exception of one transition with a residual of 430 kHz. Table 2 illustrates the effects

Table 2

Rotational, centrifugal distortion constants and determinable combinations of coefficients^a for the 6^1 and 7^1 vibrational states from analyses with and without Coriolis interactions included

	Ground state ^b /MHz	Without Coriolis interaction		With Coriolis interaction	
		7^1	6^1	7^1	6^1
		Change from GS/MHz		Percent change from GS	
A	13012.26285	16.10	-21.03	15.74	-21.02
B	12096.924	-1.10	-41.70	-0.75	-41.70
C	6260.137183	-57.23	77.01	-17.52	-2.41
	Ground state ^b /kHz ^c	Percent change from GS		Percent change from GS	
Δ_J	8.901231	-0.5	9.8	3.5	5.7
Δ_{JK}	-4.49804	-32.9	69.6	34.7	0.0
Δ_K	7.33846	-16.4	28.8	20.0	-9.1
δ_J	3.782612	9.0	0.9	4.3	5.6
δ_K	7.49446	6.4	3.6	7.5	2.2
T_{aa}	-11.74166	2.0	-1.2	1.9	-1.3
T_{bb}	-16.46654 ^d	3.9	5.7	3.9	5.6
T_{cc}	-1.336007	-54.3	60.5	-0.6	6.6
T_1	-22.20565	6.1	-2.3	-2.8	6.9
T_2	-172.11832	3.8	-1.4	-5.1	7.9

^a See Table 2 in Ref. [13] for relationships between the distortional constants and the determinable combinations of coefficients.

^b Ground state constants are from Ref. [5].

^c The units for T_2 are MHz².

^d In Ref. [13], -6.47697 should be -16.47697.

The ratio of the moment of inertia of the top to that of the frame, ρ , cannot be fit for in SPFIT and was empirically adjusted to minimize the *rms* deviation of the fit. We used the convention that the NO₂ group was the top and OH the frame that allowed for a more convenient labeling of the states in SPFIT. Table 1 summarizes the measurements that include 1193 transitions that extend to maximum quantum numbers of $J = 73$ and $K_a = 59$. The *rms* deviation of fit was 87 kHz and a comparison of the fitted constants with the other vibrational states was not attempted due to the use of the IAS Hamiltonian. When comparing the torsional parameters between the two isotopologues, the structural parameter ρ was unchanged and there was only a slight change in the torsional splitting parameter E_ρ which changed from 1.170(4) MHz for H¹⁴NO₃ to 1.213(3) MHz for H¹⁵NO₃. For the D¹⁴NO₃ isotope, the torsional splitting for the 9¹ state is not resolvable [28].

3.4. 5¹ and 9² state analysis

The ν_5 vibrational mode corresponds to the NO₂ in plane bend and is centered near 871 cm⁻¹, shifted down by ~8 cm⁻¹ from the main isotopic species, while the $2\nu_9$ is associated with the O–H torsional mode and is centered near 893 cm⁻¹, shifted down by ~3 cm⁻¹ from the main isotopic species [9,10]. The difference in the band origins is ~22 cm⁻¹ (compared to ~17 cm⁻¹ for the normal species) and these two states are coupled via a strong Fermi resonance that must be fit for simultaneously since this strong resonance causes the 5¹ and 9² wavefunctions to be mixed. In the infrared, this mixing results in an intensity borrowing where the expected weak $2\nu_9$ overtone band and expected strong ν_5 fundamental band have an unexpectedly large intensity ratio of $\text{Int}(2\nu_9)/\text{Int}(\nu_5) \sim 0.23$ [9]. For pure rotational transitions, the mixing results in an induced torsional splitting observed for the 5¹ lev-

els that would normally be expected only for the 9² levels. The observed torsional splitting is ~70 MHz for the 9² state rotational transitions and ~15 MHz for the 5¹ state transitions. Assuming the splitting in the 5¹ transitions is due to the wavefunction mixing, then the percent mixing is ~82% to ~18%, which then predicts the intensity ratio of 0.214 for the infrared bands, which is in close agreement with the observed ratio.

Due to the torsional splitting, the IAS Hamiltonian was used to fit the 5¹/9² states and follows the “induced splitting” model from Ref. [12] where the zero-order Fermi resonance term, F_0 , was fit for and only the 9² state was given a set of torsional parameters. The torsional splitting in the 5¹ state is then completely accounted for through the mixing of the wavefunctions due to the Fermi resonance rather than fitting for a separate set of torsional parameters. The Fermi operators coupling the vibrational states are given by

$$H_{vv'}^F = F_0 + F_J J^2 + F_K J_a^2 + 2F_{\pm} J_{bc}^2 + 2F_{\pm K} \{J_a^2, J_{bc}^2\} \quad (7)$$

and the resulting mixing of the vibrational wavefunctions can be expressed as

$$a^2 = \frac{1}{2} \left(1 + \sqrt{1 - \frac{4F_0^2}{\Delta E^2}} \right) \quad (8)$$

where the coefficient a^2 represents the fractional mixing and ΔE is the difference in the observed (perturbed) band origins. The Coriolis interaction operators are given by Eq. (3).

Table 1 summarizes the measurements that include 544 transitions that extend to maximum quantum numbers of $J = 60$ and $K_a = 41$ for the 5¹ state and 581 transitions that extend to maximum quantum numbers of $J = 60$ and $K_a = 40$ for the 9² state with transitions measured up to a maximum frequency of 655 GHz. Due to localized anharmonic $\Delta K_a = \pm 2$ resonances, 79 transitions were labeled as interstate rovibrational transitions and are listed in

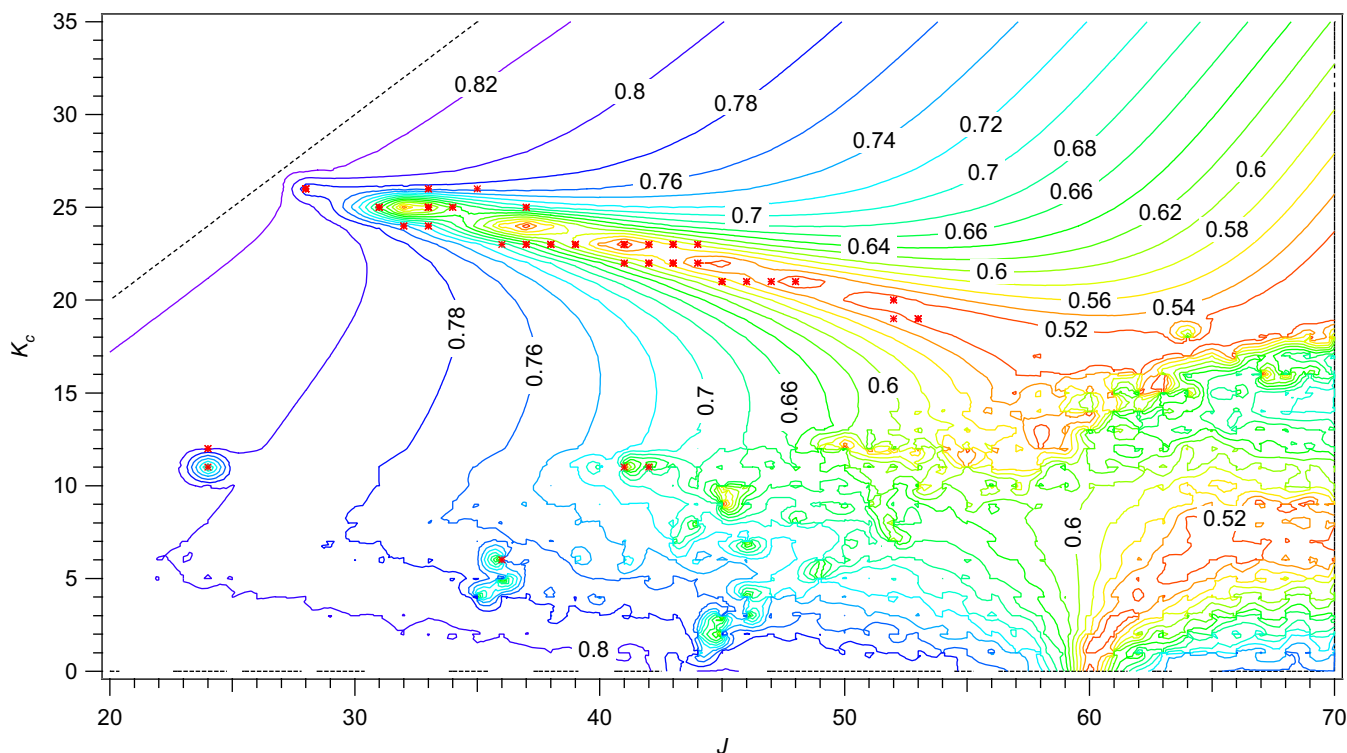


Fig. 2. A contour plot of the vibrational wavefunction mixing coefficients as a function of quantum number for the $\nu_5 = 1$ state. Note the base mixing coefficient of ~82% due to the F_0 term coupling the states. The variation in the contours arise due to local resonances and the levels involved in the interstate rovibrational transitions are labeled with the * symbol.

Table 3. Fig. 2 provides a contour map of the wavefunction mixing for the 5^1 levels along with the 5^1 state energy levels involved in the interstate rovibrational transitions.

The observed torsional splitting in each state is directly related to the mixing and the rotational transitions allow both the zero-order Fermi term, F_0 , and the difference in the band origins, ΔE , to be determined. However, since F_0 is highly correlated with the vibrational energies E_5 and E_{99} and pure rotational transitions do not depend directly on these energies, we included the band origins reported by Perrin and Mbiaké [9] in the analysis as 'measured rotationless transitions' with values of 871.0955(3) and 893.4518(3) cm^{-1} for the ν_5 and $2\nu_9$ bands, respectively, where the uncertainty in parenthesis reflects the estimated systematic uncertainty. This allowed both band origins and the zero-order Fermi term to be fit for simultaneously. Excluding one of these bands centers from the analyses does not significantly change the fitted parameters since the rotational transitions provided sufficient information to determine both the F_0 and $\Delta E = E_{99} - E_5$, even though these remain highly correlated (correlation coefficient of -0.999996). As demonstrated in Ref. [10] for H^{14}NO_3 , the statistical uncertainty in these correlated parameters can be reduced if all the measured infrared energy levels are included in the analysis. When comparing the F_0 parameter for H^{15}NO_3 to that determined for H^{14}NO_3 in Refs. [10,12], this parameter is only slightly higher ($\sim 0.2\%$) and is not significantly different. If the band origins are fixed at the values reported in Ref. [9], the uncertainty in the F_0 terms is reduced by a factor of 300 to a value of 255738.055(96) MHz without significant changes in the other constants or the analysis. However, this value is still highly dependent on the band origins.

The torsional splitting parameter, E_ρ , determined for the 9^2 states for each isotopologue are nearly identical with values of 43.04(1) MHz for H^{15}NO_3 and 43.15(1) MHz for H^{14}NO_3 reported in a similar analysis in Ref. [12]. While the infrared analysis for the $5^1/9^2$ dyad of H^{15}NO_3 in Ref. [9] did not require the non-orthorhombic terms, such as $D_{ab}^v \{J_a, J_b\}$, they were required in this analysis to describe the interaction between the torsional sublevels (Wang submatrices, $E^\pm \leftrightarrow O^\pm$), which is significant when the torsional splitting is approximately equal to the asymmetry splitting.

4. Summary

The rotational spectrum of H^{15}NO_3 has been recorded in the range between 74 and 850 GHz. The spectrum of the six lowest lying vibrational states (9^1 , 7^1 , 6^1 , 8^1 , 5^1 , and 9^2) have been analyzed and fit to produce a set of spectroscopic parameters that accurately predict the thermally populated millimeter and submillimeter wave spectrum over this range of frequencies. Fermi and Coriolis interactions between various states have been accounted for as well as the torsional splitting of the 9^1 , 9^2 and 5^1 states.

Acknowledgments

The authors thank Frank C. De Lucia for use of the FASSST spectrometer and other resources in the Microwave Laboratory at Ohio State University. This material is based upon work supported by NASA, partially supported by the NSF under Grant No. 0353963 and through funding provided by the Department of Defense.

Portions of this paper present research carried out at the Jet Propulsion Laboratory, California Institute of Technology, under contract with the National Aeronautics and Space Administration. Any opinions, findings, and conclusions or recommendations expressed in this material are those of the author(s) and do not necessarily reflect the views of NASA.

Appendix A. Supplementary data

Supplementary data for this article are available on ScienceDirect (www.sciencedirect.com) and as part of the Ohio State University Molecular Spectroscopy Archives (http://library.osu.edu/sites/msa/jmsa_hp.htm). Supplementary data associated with this article can be found, in the online version, at [doi:10.1016/j.jms.2008.03.025](https://doi.org/10.1016/j.jms.2008.03.025).

References

- [1] M.L. Santee, W.G. Read, J.W. Waters, L. Froidevaux, G.L. Manney, D.A. Flower, R.F. Jarnot, R.S. Harwood, G.E. Peckham, *Science* 267 (1995) 849–852.
- [2] A. Perrin, J.-M. Flaud, R. Mbiaké, G.G. Brizzi, M. Carlotti, M. Ridolfi, in: 61st International Symposium on Molecular Spectroscopy, Ohio State University, Columbus, OH, USA, 2006.
- [3] T.B. Coplen, J.K. Bohlke, P. De Bièvre, T. Ding, N.E. Holden, J.A. Hopple, H.R. Krouse, A. Lamberty, H.S. Peiser, K. Revesz, S.E. Rieder, K.J.R. Rosman, E. Roth, P.D.P. Taylor, R.D. Vocke, Y.K. Xiao, *Pure Appl. Chem.* 74 (2002) 1987–2017.
- [4] D.J. Millen, J.R. Morton, *J. Chem. Soc.* (1960) 1523–1528.
- [5] B.J. Drouin, C.E. Miller, J.L. Fry, D.T. Petkie, P. Helminger, I.R. Medvedev, *J. Mol. Spectrosc.* 236 (2006) 29–34.
- [6] G.E. McGraw, D.L. Bernitt, I.C. Hisatsune, *J. Chem. Phys.* 42 (1965) 237–244.
- [7] W.F. Wang, P.P. Ong, H.F. Chen, H.H. Teo, *J. Mol. Spectrosc.* 185 (1997) 207–208.
- [8] F. Keller, A. Perrin, J.-M. Flaud, J.W.C. Johns, Z. Lu, E.C. Looi, *J. Mol. Spectrosc.* 191 (1998) 306–310.
- [9] A. Perrin, R. Mbiaké, *J. Mol. Spectrosc.* 237 (2006) 27–35.
- [10] A. Perrin, J. Orphal, J.-M. Flaud, S. Klee, G. Mellau, H. Mader, D. Walbrodt, M. Winnewisser, *J. Mol. Spectrosc.* 228 (2004) 375–391.
- [11] D.T. Petkie, P. Helminger, R.A.H. Butler, S. Albert, F.C. De Lucia, *J. Mol. Spectrosc.* 218 (2003) 127–130.
- [12] D.T. Petkie, T.M. Goyette, P. Helminger, H.M. Pickett, F.C. De Lucia, *J. Mol. Spectrosc.* 208 (2001) 121–135.
- [13] D.T. Petkie, P. Helminger, M. Behnke, I.R. Medvedev, F.C. De Lucia, *J. Mol. Spectrosc.* 233 (2005) 189–196.
- [14] S. Albert, D.T. Petkie, R.P.A. Bettens, S.P. Belov, F.C. De Lucia, *Anal. Chem.* 70 (1998) 719A–727A.
- [15] I. Medvedev, M. Winnewisser, F.C. De Lucia, E. Herbst, E. Bialkowska-Jaworska, L. Pszczolkowski, Z. Kisiel, *J. Mol. Spectrosc.* 228 (2004) 314–328.
- [16] D.T. Petkie, T.M. Goyette, R.P.A. Bettens, S.P. Belov, S. Albert, P. Helminger, F.C. De Lucia, *Rev. Sci. Instrum.* 68 (1997) 1675–1683.
- [17] B.J. Drouin, F.W. Maiwald, J.C. Pearson, *Rev. Sci. Instrum.* 76 (2005). Art. No.093113.
- [18] A.P. Cox, J.M. Riveros, *J. Chem. Phys.* 42 (1965) 3106–3112.
- [19] J.K.G. Watson, in: J.R. Durig (Ed.), *Vibrational Spectra and Structure*, vol. 6, Elsevier, New York, 1977, pp. 1–89.
- [20] H.M. Pickett, *J. Mol. Spectrosc.* 148 (1991) 371–377.
- [21] H.M. Pickett, R.L. Poynter, E.A. Cohen, M.L. Delitsky, J.C. Pearson, H.S.P. Muller, *J. Quant. Spectrosc. Rad. Transfer* 60 (1998) 883–890.
- [22] E.C. Looi, T.L. Tan, W.F. Wang, P.P. Ong, *J. Mol. Spectrosc.* 176 (1996) 222–225.
- [23] W. Gordy, R.L. Cook, *Microwave Molecular Spectra*, third ed., John Wiley & Sons, New York, 1984.
- [24] T.L. Tan, W.F. Wang, E.C. Looi, P.P. Ong, *Spectrochim. Acta* 52A (1996) 1315–1317.
- [25] T. Tanaka, Y. Morino, *J. Mol. Spectrosc.* 5 (1969) 436–448.
- [26] A. Goldman, J.B. Burkholder, C.J. Howard, R. Escibano, A.G. Maki, *J. Mol. Spectrosc.* 131 (1988) 195–200.
- [27] L.H. Coudert, A. Perrin, *J. Mol. Spectrosc.* 172 (1995) 352–368.
- [28] S.G. Chou, D.T. Petkie, R.A.H. Butler, C.E. Miller, *J. Mol. Spectrosc.* 211 (2002) 284–285.